Numerical investigation of edge plasma phenomena in an enhanced D-alpha discharge at Alcator C-Mod: Parallel heat flux and quasi-coherent edge oscillations

D. A. Russell, D. A. D'Ippolito, J. R. Myra, B. LaBombard, J. L. Terry, and S. J. Zweben

Citation: Physics of Plasmas (1994-present) **19**, 082311 (2012); doi: 10.1063/1.4747503
View online: http://dx.doi.org/10.1063/1.4747503
View Table of Contents: http://scitation.aip.org/content/aip/journal/pop/19/8?ver=pdfcov
Published by the AIP Publishing

Numerical investigation of edge plasma phenomena in an enhanced D-alpha discharge at Alcator C-Mod: Parallel heat flux and quasi-coherent edge oscillations

D. A. Russell,[1,a)] D. A. D'Ippolito,[1] J. R. Myra,[1] B. LaBombard,[2] J. L. Terry,[2] and S. J. Zweben[3]
[1]*Lodestar Research Corporation, 2400 Central Ave., P-5, Boulder, Colorado 80301, USA*
[2]*Plasma Science and Fusion Center, Massachusetts Institute of Technology, 167 Albany Street, Cambridge, Massachusetts 02138, USA*
[3]*Princeton Plasma Physics Laboratory, P.O. Box 451, Princeton, New Jersey 08540, USA*

(Received 2 May 2012; accepted 7 August 2012; published online 20 August 2012)

Reduced-model scrape-off layer turbulence (SOLT) simulations of an enhanced D-alpha (EDA) H-mode shot observed in the Alcator C-Mod tokamak were conducted to compare with observed variations in the scrape-off-layer (SOL) width of the parallel heat flux profile. In particular, the role of the competition between sheath- and conduction-limited parallel heat fluxes in determining that width was studied for the turbulent SOL plasma that emerged from the simulations. The SOL width decreases with increasing input power and with increasing separatrix temperature in both the experiment and the simulation, consistent with the strong temperature dependence of the parallel heat flux in balance with the perpendicular transport by turbulence and blobs. The particularly strong temperature dependence observed in the case analyzed is attributed to the fact that these simulations produce SOL plasmas which are in the conduction-limited regime for the parallel heat flux. A persistent quasi-coherent (QC) mode dominates the SOLT simulations and bears considerable resemblance to the QC mode observed in C-Mod EDA operation. The SOLT QC mode consists of nonlinearly saturated wave-fronts located just inside the separatrix that are convected poloidally by the mean flow, continuously transporting particles and energy and intermittently emitting blobs into the SOL. © *2012 American Institute of Physics*.
[http://dx.doi.org/10.1063/1.4747503]

I. INTRODUCTION

First observed and routinely reproduced at Alcator C-Mod ever since, the enhanced D-alpha high-confinement mode (EDA H-mode)[1–3] provides an interesting approach to sustain good confinement necessary for reactor-scale operation. The EDA H-mode gets its name from the enhanced D_α emission (relative to that of the conventional H-mode). It is not plagued by edge-localized modes (ELMs), yet it does not suffer the radiative collapse (and subsequent relaxation to the low-confinement mode, or L-mode) that typically curtails the ELM-free H-mode. The mode owes its freedom from radiative collapse to its enhanced particle transport, which occurs by a continuous (i.e., not an intermittent) process. The enhanced particle transport reduces impurity build-up in the core while energy confinement time remains comparable to that of the ELM-free H-mode.

From a practical point of view, it is important to understand how the parallel heat flux in the scrape-off layer (SOL) scales with characteristic parameters of the EDA in order to anticipate operational constraints on future machines that may attempt to run scaled-up versions of this operational mode. Practical concerns include damage to the divertor and other plasma-facing components, main-chamber wall recycling, and power-exhaust control.[4] Such concerns tend to focus attention on the radial profile of the parallel heat flux in the SOL as a function of the power entering the SOL (P_{SOL}) in the outboard midplane (OM) region. In particular, the rate with which that profile falls off with increasing radius, i.e., the "SOL width," is determined by the competition between perpendicular transport into, and parallel energy transport away from, the OM.

Perpendicular turbulent transport and its effect on SOL profiles have been addressed previously. Earlier work by other authors compared the turbulent radial transport of density and temperature obtained from ESEL code simulations[5] with experimental data for TCV (Refs. 6 and 7) and JET.[8] These studies obtained reasonable agreement between simulation and experimental SOL profiles and demonstrated that radial transport of both particles and energy were dominated by turbulent motions of plasma blob-filaments. The SOL heat-flux width scaling was not explicitly addressed.

The present paper presents results from reduced-model, scrape-off layer turbulence simulations of an EDA H-mode shot at C-Mod. The simulations were carried out using the SOLT code.[9] It was motivated by (and closely adopts the methods of) a previous study[10] of the SOL heat-flux width in low-power H-mode discharges at NSTX. Interesting differences were found between the scalings in the two simulations (for the NSTX and C-Mod cases) that shed light on the underlying physics in the experiments.

In SOLT simulations, blobs of plasma are generated by the nonlinear saturation of the interchange instability in the edge region of the OM.[9] Unchecked, the (charge-polarized)

a)Electronic mail: dave@lodestar.com.

blobs would $\mathbf{E}\times\mathbf{B}$-stream radially outward into the SOL,[11,12] in SOLT's version of the L-mode. However, in these H-mode simulations, consistent with experimental measurements[4] and general theoretical considerations,[13] there is a quasi-stationary, sheared, mean poloidal flow that acts as a transport barrier, bottling-up the blobs in a neighborhood of the separatrix, near a local maximum (i.e., zero-shear point) of the flow. In a frame moving with this local flow maximum, the density blobs are quasi-stationary. But to each blob is associated a local dipole vorticity (or charge). This row of poloidally streaming, separatrix-spanning vortices[10] is responsible for the radial transport of energy and particles into the near-SOL in the H-mode simulations for both NSTX and Alcator C-Mod, although the vortices are more intermittent in NSTX than in C-Mod. The quasi-stationary vortices give the EDA H-mode the appearance of a continuous process, consistent with the earliest observations at Alcator C-Mod.[2]

There are significant *quantitative* differences between the transport characteristics of the two experiments. For example, the parallel heat flux width *decreases* with increasing P_{SOL} in the C-Mod EDA H-mode shot, while it *increases* with increasing power in a series of NSTX H-mode shots studied earlier.[10] The SOLT simulations reproduce these observations, and analysis of the simulations suggests that the explanation for the observed difference in SOL width scaling lies in the greater collisionality of the C-Mod shot, which we will discuss in Sec. III.

In the simulations of the EDA H-mode, the string of blobs, streaming by at the local poloidal mean-flow velocity, generates a strong quasi-coherent feature in power spectra of the density fluctuations. Similarly, the energy spectrum peaks at a wave number ($\sim 1\,\mathrm{cm}^{-1}$) determined by the average number of blobs per unit poloidal length in the string. These spectral features are like those associated with the quasi-coherent (QC) mode[4] that is invariably observed during EDA operation at C-Mod. We explore SOLT's QC mode in Sec. IV.

II. THE SIMULATION MODEL

A. Equations of evolution

The SOLT model equations have been elucidated previously. Here we briefly recapitulate the description given in Refs. 9 and 10 for completeness. The work in Ref. 10 strongly motivated the present investigation, and we adopt its methodology and notations, but not its parameters, here. Our choice of parameters and profiles for simulating the EDA H-mode is described next in Sec. II B.

SOLT is a two-dimensional (2D) electrostatic fluid turbulence code. The code models the evolution of potential, density, and temperature in a plane perpendicular to the magnetic field B, in the OM region of the torus. The potential evolution is described in terms of the evolution of fluctuating (i.e., poloidally varying) vorticity and mean (i.e., poloidally averaged) fluid momentum. SOLT contains a reduced description of the electron drift wave and interchange instabilities and sheath physics. Curvature- and grad-B-driven charge polarization enable blob transport of strong fluctuations ($\delta n/n \sim 1$) from the edge into the SOL. The parallel physics is modeled by closure schemes which depend upon the regime.[14] The code has recently been generalized to allow regime-dependent closures for the parallel current and heat flux.[10]

The basic equations of the SOLT model in dimensionless form (using the Bohm normalization with reference time-scale $\Omega_{ci}^{-1} = [ZeB/m_i c]^{-1}$ and space-scale $\rho_{sr} = c_{sr}/\Omega_{ci}$ where $c_{sr}^2 = T_{er}/m_i$ and T_{er} is a reference temperature for the normalization) are

$$\frac{\partial}{\partial t}\nabla^2\tilde{\Phi} + \{v\cdot\nabla\nabla^2\Phi\} = \left\{\alpha_{dw}\frac{\bar{T}^{3/2}}{\bar{n}}(\Phi - T\ln n) + \alpha_{sh}\frac{J_{\parallel}}{n} - \frac{\beta}{n}\frac{\partial(nT)}{\partial y} + \mu\nabla^4\Phi\right\}, \tag{1}$$

$$\frac{dn}{dt} = \alpha_{dw}\bar{T}^{3/2}\{\Phi - T\ln n\} - \alpha_{sh}(nT^{1/2} - J_{\parallel}) + D_n\nabla^2 n + S_n, \tag{2}$$

$$\frac{dT}{dt} = -\alpha_{sh}\frac{q_{\parallel}}{n} + D_T\nabla^2 T + S_T, \tag{3}$$

$$\frac{\partial p_y}{\partial t} + \frac{\partial}{\partial x}\langle n v_x v_y\rangle = -\int_x^{L_x} dx\,\alpha_{sh}\langle J_{\parallel}\rangle + \bar{\mu}\frac{\partial^2}{\partial x^2}\bar{v}_y + \nu_p\cdot(p_{y0} - p_y). \tag{4}$$

The simulation plane is denoted as the (x, y) plane where x is the radial direction and y is bi-normal (approximately poloidal). Here, for any quantity Q, $\langle Q\rangle \equiv \bar{Q}$ denotes the y-averaged or *mean* part and $\tilde{Q} \equiv \{Q\} \equiv Q - \bar{Q}$ denotes the fluctuating part. Also, we define $\mathbf{v} = \mathbf{e}_z\times\nabla\Phi$ and $d/dt = \partial/\partial t + \mathbf{v}\cdot\nabla$. These equations evolve fluctuating vorticity $\nabla_\perp^2\tilde{\Phi}$, plasma density n, electron temperature T, and mean poloidal momentum $p_y = \langle n v_y\rangle$, where $v_y = \partial\Phi/\partial x$. The fluctuating and mean potentials ($\tilde{\Phi}$ and $\bar{\Phi}$) can then be extracted to form the total potential $\Phi = \tilde{\Phi} + \bar{\Phi}$. This approach enforces momentum conservation explicitly. The integral in Eq. (4) extends to the end of the simulation box ($x = L_x$) and describes the dissipation of momentum in the sheaths.

The parameter $\alpha_{dw} \sim 2k_{\parallel}^2 v_{te}^2/\nu_{ei}\Omega_i$ (where v_{te} is the electron thermal velocity) arises from the collisional parallel electron dynamics and, when dominant, enforces the Boltzmann relationship between density and potential fluctuations on closed field lines. Those terms which include it in the density and vorticity equations provide a model of electron drift wave dynamics.[15] It is a smooth function of radius, maximized at the core-side boundary ($x = 0$) and falling to zero in a neighborhood of the separatrix, or last closed flux surface (LCFS). The assumptions in our drift wave model are discussed in more detail at the end of this section.

The parameter $\alpha_{sh} = 2\rho_{sr}/L_{//}(x)$ is a function of radius, inversely proportional to the connection length $L_{//}(x)$, which is defined to be the shortest distance to a divertor, along an open field line, from a point (x) in the OM. The parameter α_{sh} is strictly zero inside the LCFS and, in the present work, is an increasing function of radius outside (see Fig. 1). The parameter $\beta = 2\rho_{sr}/R_c$, where R_c is the radius of curvature of

the field lines (here taken equal to the major radius of the machine), accounts for the curvature and grad-B drifts which drive the interchange instability. For the parameters of the present study, the interchange instability sustains the turbulence; if $\beta = 0$, fluctuations die away and profiles relax to quiescent limits. D_n, D_T, μ, and $\bar{\mu}$ are the diffusion coefficients for density, temperature, vorticity, and mean flow.

The simulation uses forms for the particle, energy, and momentum sources that facilitate simulation of experimental shot data. Inside the separatrix, density and temperature are restored to reference profiles using the source functions in Eqs. (2) and (3): $S_n = \nu_n(x)\cdot(n_0(x) - n)$ and $S_T = \nu_T(x)\cdot(T_0(x) - T)$, where $n_0(x)$ and $T_0(x)$ are taken from the experiment. The restoration rates $\nu_{n,T}(x)$ are maximized at the core-side boundary and fall to zero sufficiently within the LCFS that they do not affect the dynamics in the interchange instability-dominated edge and SOL regions. Similarly, in Eq. (4), we restore the mean flow to a reference flow profile $p_{y0}(x)$. In an earlier study of saturation mechanisms in L-mode turbulence,[16] p_{y0} was taken to be identically zero, and v_p was taken to be a constant that was varied to control the flow shear. As in the H-mode study that motivated this one,[10] we take $p_{y0}(x)$ to be a non-trivial prescribed flow and relax to it only inside the LCFS, i.e., $v_p(\mathrm{SOL}) = 0$, so the poloidal momentum evolution is self-consistent in the SOL but constrained inside the LCFS. The choice of p_{y0} is described in Sec. II B below. In summary, the simulation is designed to evolve self-consistent physical dynamics in the SOL but is constrained to connect smoothly to prescribed (i.e., experimentally measured) quantities for the simulated discharge in the core region.

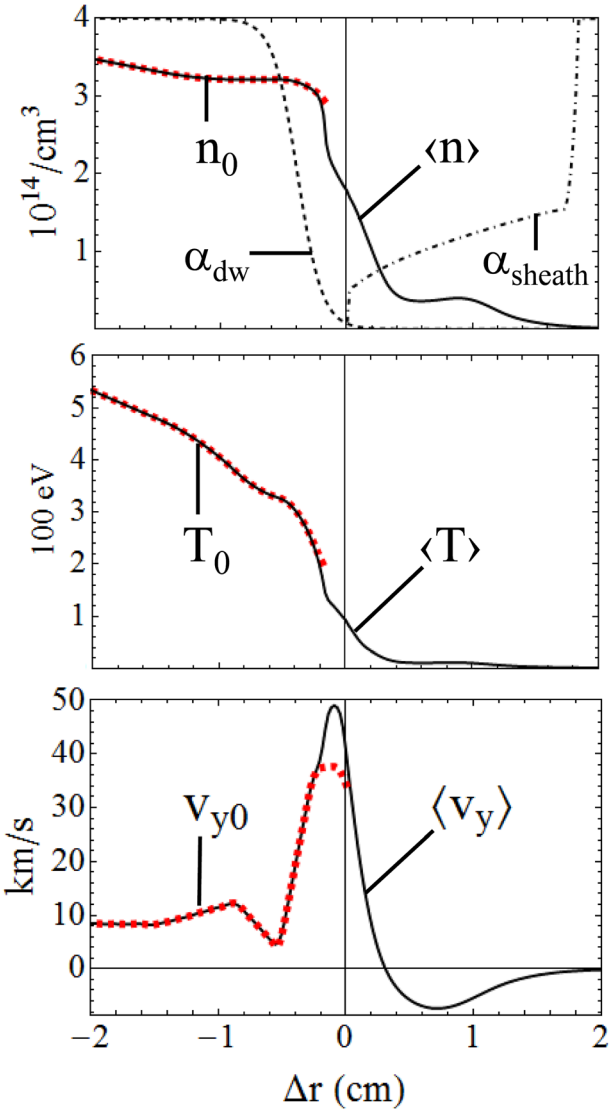

FIG. 1. Reference density (n_0) and electron temperature (T_0) profiles from the first time-slice (1.052 s) at C-mod and the inferred mean poloidal flow [see Eq. (13)] (v_{y0}) are shown as dashed lines on the core-side ($\Delta r < 0$) of the separatrix ($\Delta r = 0$). The radial electric field well characteristic of the H-mode is proportional to $-(v_{y0})$ in our model. Profiles from the best power-matched SOLT simulation for this time-slice ($\tau = 2.2$) are the solid curves. Re-scaled adiabaticity (α_{dw}) and sheath (α_{sheath}) profiles are plotted in the density panel. Angular brackets denote temporal (t) and poloidal (y) averages.

To close the system of equations, the parallel current $J_\parallel$ and heat flux $q_\parallel$ must be expressed in terms of the dynamic variables Φ, n, and T. We recently implemented a set of closure relations, valid for a range of collisionality regimes, from conduction-limited to sheath-connected, as discussed in Appendix A of Ref. 10. The low collisionality limit of these expressions recovers the sheath connected limit used in previous work.

The dimensionless forms of the parallel heat flux in the sheath-limited (SL), flux-limited (FL), and conduction-limited (CL) regimes are

$$q_{\parallel \mathrm{SL}} = s_E\, n T^{3/2} e^{(\Phi_B - \Phi)/T}, \tag{5}$$

$$q_{\parallel \mathrm{FL}} = C_{\mathrm{fle}}\, n T^{3/2}, \tag{6}$$

$$q_{\parallel \mathrm{CL}} = \frac{3.2 n T^{3/2}}{\Lambda} = \frac{3.2 T^{7/2}}{\Lambda_r}\frac{\alpha_{sh}}{\alpha_{sh0}}. \tag{7}$$

Here $\Phi_B \sim 3\,T_e$ is the Bohm sheath potential, α_{sh0} is the value of α_{sh} at a reference value of connection length $L_\parallel$, and the dimensionless collisionality parameter is given by $\Lambda = \nu_{ei} L_\parallel/(\Omega_e \rho_s)$, with Λ_r evaluated at reference parameters to underscore the temperature dependence of $q_{\parallel \mathrm{CL}}$. The flux limit for electron heat conduction is $C_{\mathrm{fle}} = 60 \sim (m_i/m_e)_{1/2}$. A smooth interpolation between regimes is given by

$$1/q_\parallel = 1/q_{\parallel\,\mathrm{SL}} + 1/q_{\parallel\,\mathrm{FL}} + 1/q_{\parallel\,\mathrm{CL}}\,, \tag{8}$$

and we adopt this expression in the simulations. The smallest of $q_\parallel$'s components dominates the result. As collisionality is raised, the system transitions from sheath-limited to conduction-limited.

For the parallel current, a similar method (i.e., piecing together asymptotic results from the different regimes) is employed, with

$$1/J_\parallel = 1/J_{\parallel\,\mathrm{SL}} + \Theta(\Phi_B - \Phi)/J_{\parallel\,\mathrm{eFL}} + 1/J_{\parallel\,\mathrm{CL}}\,, \tag{9}$$

where $\Theta(\Phi_B - \Phi)$ is the Heavyside step-function and the following expressions, similar to Eqs. (5)–(7), hold for the components of $J_\parallel$ in the corresponding regimes.[10]

$$J_{\parallel SL} = nT^{1/2}\left(1 - e^{(\Phi_B - \Phi)/T}\right), \tag{10}$$

$$J_{\parallel eFL} = -C_{fle}\, nT^{1/2}, \tag{11}$$

$$J_{\parallel CL} = 1.96\frac{T^{5/2}}{\Lambda_r}\frac{(\Phi - \Phi_B)}{T}\frac{\alpha_{sh}}{\alpha_{sh0}}. \tag{12}$$

Here, as discussed in Ref. 10, Φ_B is regarded as a free order-unity parameter taken to be 3 in the present work. We emphasize that Eqs. (8) and (9) depend on the evolving fields, so that the turbulent evolution self-consistently determines the collisionality regime.

B. Parameters and profiles

The parameters and profiles for the simulations are taken from the experiment: EDA H-mode shot #1100303018 at Alcator C-Mod, measured at 1.052 and 1.409 s into the shot. For each of these two time slices, we use the measured density and temperature profiles, from the C-Mod edge Thomson scattering system, as our reference profiles (n_0 and T_0). The dimensionless profiles used in the code are the physical versions divided by their values at the LCFS, and the reference values for length (ρ_{sr}) and velocity (c_{sr}) used to convert between physical and dimensionless variables are similarly measured at the separatrix for each time slice. The reference profiles are plotted in Fig. 1 for the earlier time slice. (We use "x" and "Δr" to denote the radial dimension, but the origin for Δr is the location of the separatrix: $\Delta r \equiv x - x_{SEP}$.)

The magnetic induction is 4 T, and this is a deuterium plasma, so that $\Omega_{ci} = 1.9 \times 10^8$ rad/s. The reference quantities are $T_{er} = 117.4$ eV, $\rho_{sr} = 0.39$ mm, and $c_{sr} = 75$ km/s at the first time slice; $T_{er} = 86$ eV, $\rho_{sr} = 0.34$ mm, and $c_{sr} = 64$ km/s at the second (radiated power was higher in the 2nd time slice, leading to lower T_e at the LCFS). It follows from this temperature dependence that $\beta = 2\rho_{sr}/R = 8.75 \times 10^{-4}$ and 7.5×10^{-4}, at the two slices ($R_c \approx R = 89.5$ cm).

The connection length, $L_{//}(x)$, is obtained from the MHD equilibrium code EFIT at each of the two time slices, and we linearly interpolate its reciprocal onto the simulation grid as the sheath absorption (or *conductivity*) coefficient, $\alpha_{sh} = 2\rho_{sr}/L_{//}(x)$, which is plotted in Fig. 1. The sudden jump in α_{sh} at $x \cong 2$ cm corresponds to the shadow of a limiter at C-Mod.

The drift wave coefficient, $\alpha_{dw}(x) = (1 - \tanh(x - x_0)/\Delta) \times 2\rho_{sr}{}^2\Omega_e/(L_{//e}{}^2 \nu_{ei0})$, decreases rapidly as the edge is approached from the core side, reflecting the increase in field line length due to the X-point, the drop in T and corresponding rise in collisionality. The electron-ion collision rate, ν_{ei0}, is calculated for reference parameters at the LCFS, and we take $1/k_\parallel \sim L_{//e} \sim qR$ with local "safety factor" $q \sim rB/RB_\theta = 3.5$, $\Delta = 5\ \rho_{sr}$, and $x_0 = 10\ \rho_{sr}$.

Recently, the role of three-dimensional (3D) effects on blob-filaments has been examined.[17] It has been shown that parallel electron physics and the resulting drift wave turbulence can alter the dynamics of blobs from that predicted by 2D interchange models. Although the present model is 2D, we attempt to incorporate some effects of drift wave dynamics on the basic interchange-ballooning mode. Satisfactory modeling of both the long-parallel wavelength blob filament ejected by interchange forces, and secondary instabilities due to the fastest growing drift wave[18] at other, generally shorter, parallel wavelengths, is not possible in our 2D simulations. For a 2D model, it is reasonable to choose $L_{\parallel e}$ in the drift-wave coefficient on the order of the longest wavelength interchange-ballooning mode ($\sim$qR) that is supported on closed surfaces. This choice yields drift waves that couple non-trivially to the interchange-ballooning mode: Linear analyses of the reference and turbulent profiles reveal unstable drift-interchange radial eigenmodes that overlap the near-SOL for which drift-wave physics clearly cannot be ignored, despite the exponential fall-off of $\alpha_{dw}(x)$ there (see Sec. V). Finally, as an additional caveat for the 2D model, note that an unambiguous translation of the magnetic field topology, e.g., safety factor and triangularity, of the experiment into the scale lengths ($L_{//e}$, Δ, and x_0) employed in the 2D model here is not possible.

The diffusion coefficients, D_n, D_T, μ, and $\bar{\mu}$, are challenging to infer directly from experiment. In the simulations, D_n, D_T, and μ are taken large enough to limit fluctuation spatial scales to a few ρ_{sr}, since smaller fluctuations are outside the purview of the SOLT model. The mean-flow viscosity coefficient, $\bar{\mu}$, is related to the vorticity diffusion coefficient, μ, by an average over the poloidal dimension, so that physical conditions outside of the OM contribute to it, in principle. As the simulation turbulence scales are unknown *ab initio*, some trial-and-error is necessary to choose these parameters. We use $(D_n, D_T, \mu, \bar{\mu}) = (0.001, 0.001, 0.2, 0.1)$ for all simulations reported here. Larger values of D_n increase the SOL width, bringing it closer to the experimental value (see Table I). But we chose a minimal-diffusion regime to emphasize the role of turbulent convection (blobs), as opposed to *ad hoc* linear diffusion, in establishing the SOL width.

The relaxation rates for the density and temperature sources (ν_n and ν_T) are chosen to restore the reference profiles smoothly near the core-side boundary ($x = 0$), without interfering with the *self-consistent* turbulent dynamics in the edge and SOL. These rates are shaped like their corresponding reference profiles, i.e., $\nu_n(x) = \nu_{n0} \cdot n_0(x)/n_0(x = 0)$ and $\nu_T(x) = \nu_{T0} \cdot T_0(x)/T_0(x = 0)$, if $x < x_{SEP} - 4\ \rho_{sr}$ and equal to

TABLE I. Power and temperature scaling of the SOL width λ_q for the EDA H-mode shot at Alcator C-Mod and for the corresponding power-matched SOLT simulations. Power matching is achieved by adjusting the parameter τ in Eq. (13). The power scan for the first time slice is shown in Fig. 2.

Time (s) C-Mod	P_{SEP} (MW) C-Mod	P_{SEP} (MW) SOLT	T_e (eV) C-Mod	T_e (eV) SOLT	λ_q (mm) C-Mod	λ_q (mm) SOLT
1.052	1.79	1.92	117	93	1.31	0.46
1.409	1.39	1.27	86	67	2.27	0.55

zero otherwise. v_{n0} and v_{T0} are equal to 0.01 in these simulations.

The momentum profile to which the mean flow relaxes *only inside the* LCFS is

$$p_{y0} = -\tau \frac{d}{dx}(n_0 T_0). \tag{13}$$

The corresponding velocity is $v_{y0} = p_{y0}/n_0$ (see Eq. (4)). Setting $\tau = T_i/T_e$ recovers the expression for the poloidal $\mathbf{E}\times\mathbf{B}$ flow that results from balancing the radial electric field force against the pressure gradient for ions. This balance is known to approximate the radial equilibrium in the H-mode pedestal.[19] Here, however, we treat τ as a free parameter and adjust it to control the turbulence by controlling the shear rate of the mean flow (and so the interchange instability, for example) in the edge region. The relaxation rate, ν_p, in Eq. (4) is equal to one if $x \le x_{SEP}$ and equal to zero otherwise. The reference flow v_{y0} is plotted in Fig. 1 as a dashed curve for $x < x_{SEP}$ along with the time-averaged SOLT equilibrium flow for the first time slice.

The simulations are on a rectangular domain, $(L_x, L_y) = (48\pi, 192\pi)\,\rho_{sr}$, resolved on a 256×512 grid. So the resolution is $(dx, dy) = (0.6, 1.2)\,\rho_{sr} = (0.23, 0.46)$ mm (the turbulence is absorbed before it can reach either radial boundary, so we show less than the full simulation radial domain in the figures). The transport algorithm is SHASTA,[20] and acceptable time-steps are bounded by a positivity constraint, similar to the Courant-Friedrichs-Lewy constraint, viz., $dt/(dx,dy) < 1/2$ maximum $(|v_x|, |v_y|)^{-1}$. All simulations are run long enough to distinguish apparent equilibria (i.e., quasi-stationary turbulence) from transient states, and time-averages are restricted to the last half of the equilibrium record.

All fields are periodic in the poloidal (y) dimension. The density and temperature are prescribed constant on the radial (x) boundaries, consistent with the reference profiles. The potential is held to the Bohm potential, 3Te, at the far-SOL boundary ($x = L_x$). The radial (x) gradient of the potential is zero there (zero poloidal mean flow at $x = L_x$) and is a specified constant (>0) at the core-side boundary ($x = 0$), consistent with the reference flow profile (see Fig. 1).

Energy spectra of fluctuations are observed to fall rapidly to ignorable levels with increasing wave number, approaching the resolution limit ($k\rho_{sr} \to 1$) and so validating the fluid model *a posteriori*. However, the discovered SOL widths, by our definition (Sec. III), are close to the reference gyro radius ρ_{sr} (~0.5 mm). So, particularly in the minimal-diffusion regime, this *diagnostic* measurement requires a radial resolution approaching the fluid limit.

III. SOL WIDTH SCALING WITH POWER AND T_e

Following Ref. 10, we calculate the power crossing the separatrix as

$$P_{SEP} = \int dA \cdot q_\perp = 2\pi R b_\theta \int dr\, q_\parallel, \tag{14}$$

where $b_\theta = B_\theta/B$, the last form uses $\nabla\cdot\mathbf{q} = 0$ (no heat sources in the SOL) and $\nabla_\parallel q_\parallel = (1/vR)(\partial q_\parallel/\partial\theta)$. Here v is a local Jacobian factor related to the global safety factor by $q = \int d\theta\, v/2\pi$, and the parallel heat flux $q_\parallel$ is calculated from the turbulent SOLT fields as in Eq. (8). Unless otherwise noted, values of P_{SEP} and radial profiles of $q_\parallel$ refer to the time- and y-average of these quantities over turbulent steady states of the simulations.

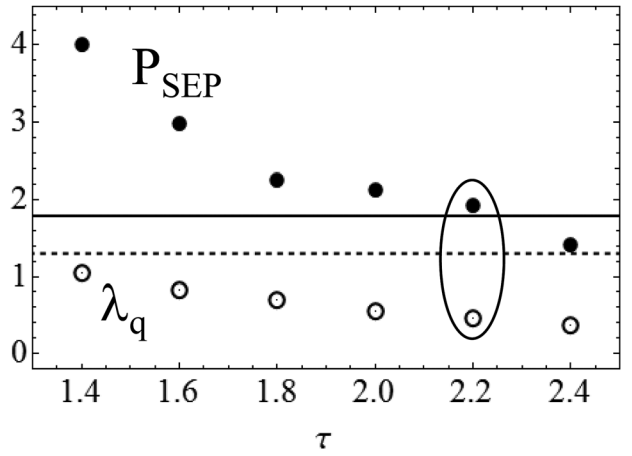

FIG. 2. P_{SEP} (filled disks) is the power (in MW) entering the SOL [Eq. (14)] at the separatrix, and λ_q (open circles) is the radial exponential decay length (in mm) of the parallel heat flux ($q_{//}$) in the near-SOL. Both are plotted as functions of the flow control parameter τ [Eq. (13)] for six SOLT simulations. Other parameters of the simulations were held fixed and chosen to model the first time-slice (1.052 s) of the C-Mod shot. The solid and dashed horizontal lines indicate the values of P_{SEP} and λ_q measured at C-Mod, respectively. The best power-matched simulation, at $\tau = 2.2$, is circled and serves as the reference simulation for this time slice.

P_{SEP} is plotted as a function of the control parameter τ in Fig. 2, along with the scale length, λ_q, from a least-squares fit of $q_\parallel$ to an exponential for $x > x_{SEP}$. The solid horizontal line indicates the value of P_{SEP} measured at the first time slice in the experiment and the dashed line indicates the measured value of λ_q. (See Fig. 4 of Ref. 4 for the histories of P_{SEP} and λ_q for the experiment. The measured values of P_{SEP} and λ_q displayed there are allowed a 20% error.) Power generally decreases with increasing τ, if all other parameters and profiles are held fixed; sufficiently large values of τ, and the correspondingly strong sheared flows, extinguish the turbulence. The experimental and simulated powers agree

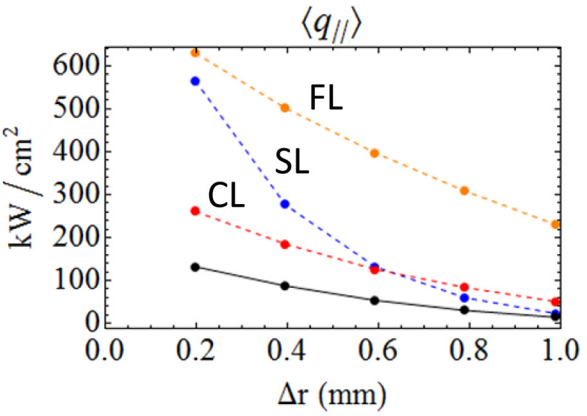

FIG. 3. The parallel heat flux, $q_{//}$ (solid), and its components (dashed): flux-limited (FL), sheath-limited (SL) and conduction-limited (CL) [see Eqs. (5)–(8)] for the reference simulation (circled in Fig. 2).

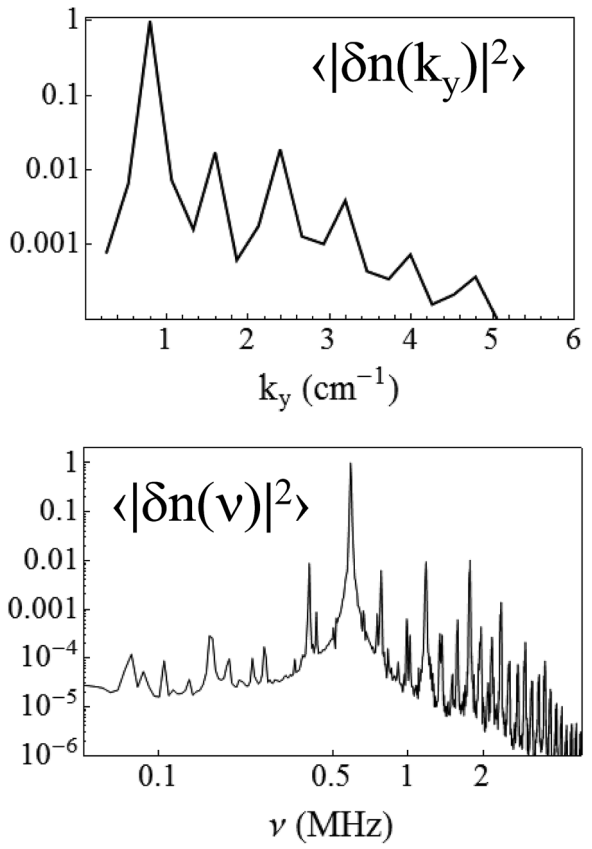

FIG. 4. Energy (k_y) and power (ν) spectra of the density fluctuations, $\delta n \equiv n\text{-}\langle n\rangle_y$, from the reference simulation, measured inside the LCFS at $\Delta r = -1.15$ mm. Each spectrum is normalized by its maximum value.

reasonably well for $\tau = 2.2$, identifying the simulation to be compared with experiment at this time slice. Similarly, $\tau = 1.6$ gives good agreement at the later time slice. We emphasize that it is important to distinguish between the power scaling for fixed edge profiles (i.e., the τ scan) and the power scaling between different experimental time slices (where both the power and the edge profiles change). The latter is the primary scaling of interest in what follows.

P_{SEP}, T_e (at the separatrix) and λ_q for the two experimental time slices and their τ-matched simulations are compared in Table I. The SOL width λ_q decreases with increasing power (and temperature at the separatrix) in both experiment and simulation. This dependence on T_e suggests that the parallel heat flux is limited by electron-ion collisions in the near-SOL in Alcator C-Mod and that this region is, therefore, relatively disconnected from the divertor sheath. Analysis of the constituents of $q_{\parallel}$ reveals this to be the case in the simulations.

The parallel heat flux and its three components (Eqs. (5)–(8)) are plotted versus radius in Fig. 3. The flux is dominated by the conduction component, $q_{\parallel CL}$, within about 0.6 mm of the separatrix. This conduction-limited flux is distinguished from the other components by the strongest dependence on temperature, $q_{\parallel CL} \sim T_e^{7/2}$ (see Eq. (7)). Higher temperature implies faster parallel transport and decreased SOL widths, least ambiguously, in this case. (The opposite scaling was observed for ELM-free H-mode shots at NSTX that are believed to have been sheath-connected in the near-SOL.[10]) Because of this strong temperature dependence, $q_{\parallel CL}$ yields to the sheath-limited $q_{\parallel SL}$ with decreasing T_e in the far-SOL, as observed in Fig. 3.

IV. SOLT'S QUASI-COHERENT MODE

A. Spatial portrait and spectral signatures

In the SOLT simulations of the EDA H-mode, there is a strong QC signal in frequency spectra of density fluctuations sampled in the edge region: a pronounced knee punctuated with several strong spikes, as shown in Fig. 4 for the P_{SEP}-matched simulation at the first time-slice. (The QC mode persists for the different τ's across the power scans.) This spectrum has a sharp maximum at $\nu_0 = 589$ kHz. The wave number spectrum, also plotted in Fig. 4, is maximized at $k_{y0} = 0.8\ \mathrm{cm}^{-1}$. Both spectra are sampled at $\Delta r = -1.15$ mm, inside the LCFS, near the maximum of mean flow (Fig. 1) at $\langle v_y\rangle = 49\ \mathrm{km/s} \cong 2\pi\,\nu_0/k_{y0}$.

The SOLT QC mode frequency (~600 kHz) is higher than that observed in the experiment (~100 kHz), likely indicating that SOLT's mean flow is about six times the mean flow in the experiment, just inside the LCFS. This difference arises because the SOLT code does not have a self-consistent model for the radial electric field, which would include the ion diamagnetic drift and toroidal geometry effects. While we are not ready to claim the SOLT QC mode is an accurate model for the QC mode observed in Alcator C-Mod EDA experiments, its surprising appearance in the simulations makes it an object well worth studying.

A snapshot of the density fluctuations is displayed in Fig. 5. The poloidal wave train, radially localized inside the LCFS, moves at the local mean flow velocity (in the electron diamagnetic drift direction) and intermittently ejects blobs into the SOL. The mean flow profile and the skewness of density fluctuations are also plotted in Fig. 5. The zero of skewness occurs where the interchange instability growth rate is maximized in a local analysis (at $\Delta r = -1.3$ mm, interpolated) and is taken as the center of the "birth zone": the radial interval where the turbulent fluctuations associated with the instability evidently originate and saturate to form blobs and holes. This picture is consistent with earlier (general as opposed to Alcator C-Mod specific) simulations[21] that did not have sheared flow.

The flow shear rate ($d\langle v_y\rangle/dx$) passes through zero in the birth zone (at $\Delta r = -1$ mm, interpolated) where the time-averaged flow velocity reaches a global maximum of 49 km/s. As flow shear is known to act as a transport barrier and to moderate the interchange instability in the birth zone, the QC mode may appear to be comprised of blobs (and holes) confined between two shear layers and drifting with the maximum mean flow. The blobs fluctuate in the co-moving frame; the stronger fluctuations result in blob emission into the SOL.

Spectral analysis of the fluctuations confirms the intrinsic Doppler nature of this QC mode. In the birth zone, the phase velocity is approximately equal to the local mean flow velocity. Moving into the high-shear region of the near-SOL, the mean flow velocity decreases, but the phase velocity of

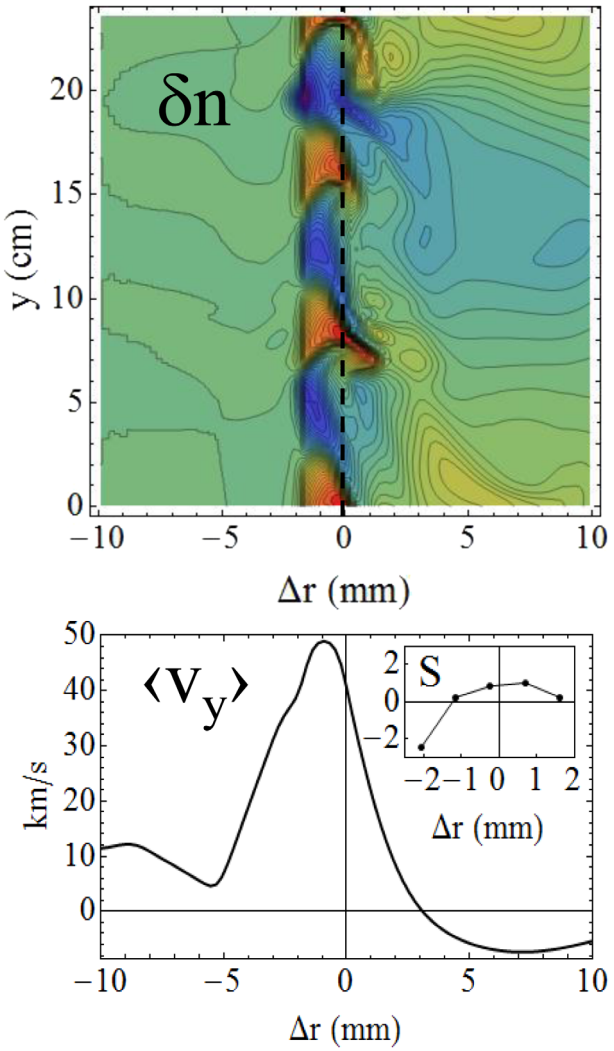

FIG. 5. The density fluctuation, $\delta n \equiv n - \langle n \rangle_y$, and the mean flow profile, $\langle v_y \rangle_{y,t}$, from the reference simulation, as functions of $(\Delta r,y)$ and of Δr respectively. The skewness of the density fluctuations (inset), $S \equiv \langle (\delta n)^3 \rangle_{y,t} / \langle (\delta n)^2 \rangle_{y,t}^{3/2}$, passes through zero in the blob "birth zone."

the mode survives from the birth zone; the passing blob string trails a wake. The spectral intensity of the QC mode diminishes with increasing radius until, beyond the flow-reversal point ($\Delta r \cong 3$ mm), the mode is absent. Density fluctuations in this far-SOL region are dominated by large ($\sim L_y/2$), downward-drifting (ion diamagnetic direction) blobs.

B. Particle flux from the SOLT QC mode

A similar, though more intermittent, saturated state was observed in a study of the ELM-free H-mode at NSTX.[10] The state was described as a poloidal train of "separatrix-spanning vortices." Here too the QC mode is comprised of separatrix-spanning vortices: each blob in the string is associated with a dipole vorticity pattern. Fluctuations about the "perfect" dipole engender net particle transport: a poloidal array of symmetric, alternating vortices transports as much plasma radially outward as inward. Although this symmetry is clearly broken in SOLT's QC mode, as blob emission demonstrates, only a small portion of the local radial particle flux results in *net* transport.

The local radial particle flux, $n \cdot v_x$ ($\equiv \Gamma$) is the sum of two pieces: a piece that is first-order in the fluctuations, $\langle n \rangle \cdot v_x$ ($\equiv \Gamma_1$), and a second-order piece, $\delta n \cdot v_x$ ($\equiv \Gamma_2$). In SOLT, the radial velocity has zero poloidal mean by definition, ($v_x = \partial\phi/\partial y$, and all fields are periodic in y, *ergo* $\langle v_x \rangle = 0$) so Γ_1 does not survive poloidal averaging while Γ_2 does and is responsible for the *net* radial transport. Γ_1 dominates power spectra sampled near the birth zone, i.e., most of the energy in the *local* radial particle flux corresponds to rotating vortices and no net transport.

We isolate that part of the net radial flux which is due to the QC mode according to

$$\langle \Gamma_2 \rangle = \Sigma' \delta n(v, k_y) \cdot v_x(v, k_y)^*,$$

a function of radius, where the angular brackets denote the time-and-poloidal average, and the summation is restricted to the QC feature in the (v,k_y)-plane. At the location of maximum flux ($\Delta r = -0.23$ mm), we find 48% of the net particle flux coming from SOLT's QC mode, in qualitative agreement with estimates from Alcator C-Mod that suggest the QC mode is a main contributor to particle transport.[3]

V. SUMMARY AND DISCUSSION

Motivated by a previous successful study of low-power H-mode discharges on NSTX,[10] we have conducted reduced-model (SOLT) simulations of the edge region of the Alcator C-Mod plasma during EDA H-mode operation. Two simulation tools, relatively new to the SOLT model, were particularly exercised in this and the preceding study: (1) Expressions for the parallel heat and particle fluxes (in the form of closure relations) allow the turbulence to adjust self-consistently between conduction-limited and sheath-limited parallel transport *in the course of evolution of the turbulence*. (2) The intensity of the turbulence is controlled by adjusting a core-side mean poloidal flow that results in strong flow shear layers in the edge.

Allowing the turbulence to adjust *self-consistently* between flux-, sheath- and conduction-limited parallel transport on open field lines, we find good agreement between simulation and experiment on the scaling of the width of the parallel heat flux radial profile ("SOL width") with power (and T_e) at the separatrix. In the SOLT simulations, the parallel heat transport is limited by *collisions* in the near-SOL for the C-Mod EDA H-mode shot, while the low-power H-modes at NSTX were observed to be sheath-limited.[10] The strong temperature dependence implied by conduction-limited parallel heat transport, $q_{//} \sim T_e^{7/2}$, is consistent with the *decrease* of SOL width with *increasing* temperature observed in the C-Mod shot and in the SOLT simulation. An opposite (but weak) scaling of SOL width with power and temperature was observed in the NSTX study where, again, experiment and simulation were in accord.[10] Thus the present SOLT model appears to be capable of producing turbulent SOL plasmas whose power width scalings adjust self-consistently to the correct collisional regime.

The SOL widths reported here are consistently smaller in the power-matched simulations than those measured in the C-Mod experiment. This discrepancy may be due to physical effects not included in the SOLT model. For example, neoclassical bulging of the plasma[22] across the separatrix may set a lower bound on the SOL width that would be enhanced by the convective transport highlighted here. We have observed that the SOL power width increases with increased linear density diffusion D_n, and typically decreases with D_T. These dependencies can be understood in light of the collisionality regime, because larger D_n and smaller D_T act to increase collisionality in the near SOL which inhibits parallel heat transport and therefore broadens the SOL. Indeed, this is the physical reason for the power scaling of λ_q discussed previously. The parameters D_n, D_T, and μ can be fine-tuned to make λ_q equal that of the experiment, but this approach lacks physical justification at this writing. Instead, the trends and qualitative features of the simulations are perhaps of greater interest.

A poloidal flow (driven by the radial electric field known to balance the ion pressure gradient during H-mode operation on both C-Mod and NSTX) was enforced at the core-side simulation boundary but evolved self-consistently with the turbulent fluctuations (Reynolds' stress) in the near-edge and SOL. While this core-side mean flow is in the electron-diamagnetic direction, the mean poloidal flow in the sheath-connected region of the SOL is in the opposite direction (determined by the Bohm potential, $\Phi_B \sim 3\,T_e$), resulting in a strong flow shear layer near the separatrix. This shear layer plays a crucial role in mediating the turbulence.

For simulations of the EDA H-mode, the turbulent saturated state consists of a poloidally arrayed train of blobs, imperfectly confined to the blob birth zone by the shear layer which intermittently allows the blobs to leak into the SOL. The poloidal convection of the blob train at the local mean flow velocity in the birth zone accounts for the quasi-coherent features observed in power spectra of the density fluctuations. This is SOLT's version of the QC mode that is the signature of the EDA H-mode at Alcator C-Mod. SOLT's QC mode maintains its birth-zone phase velocity in the SOL, out to the location where the flow reverses and the mode is lost. Isolating the mode in (ω,k_y)-space, we estimate that it accounts for approximately half of the radial particle flux near the separatrix. While we are not ready to claim the SOLT QC mode is an accurate model for the QC mode observed in Alcator C-Mod EDA experiments, its appearance in the simulations, and some qualitative and even quantitative connections to experiment, make it worthy of note.

In the course of our investigations of the SOL width, features of the turbulence came to light that beg further investigation, outside the scope of the present paper. In particular, (1) there is clear evidence of linear instabilities at work in the saturated state, and (2) there is evidence that the drift wave physics on the core side of the LCFS is associated with the observed energy cascade barrier. (Other recent work also suggests an important role for drift waves in determining blob transport.[17] However, we note that the typical blob radius in the SOL region of these simulations exceeds the R/100 limit,[17] justifying neglect of drift wave dynamics in the SOL.)

Linear analysis of the time-averaged, turbulent radial profiles reveals two branches of unstable eigenmodes in the edge region: the drift-interchange (D-I) branch, driven by curvature, and the Kelvin-Helmholtz (K-H) branch, driven by flow shear. Phase velocities on the D-I branch correspond to those of the QC mode, and the eigenfunctions are localized inside the separatrix, in the blob birth zone. The K-H eigenfunctions span the separatrix, extending farther into the SOL than the D-I eigenfunctions which they overlap. The roles of these instabilities in sustaining the turbulent fluctuations, and their respective contributions to radial transport are under investigation.

A strong maximum in the density fluctuation energy spectrum at $k_y \cong 1\,cm^{-1}$ is observed in both simulation and experiment. Cascade to the lowest poloidal mode number is not observed. As previously observed in experiment and simulation,[23] the correlation between density and potential fluctuations (i.e., the "cross-phase") shows a clear transition from interchange-dominated to drift-wave-dominated as the separatrix is crossed moving from the SOL-side into the core. The SOLT simulations reported here also show this transition in the cross-phase, in the turbulent state, near the steep turn-on of the coefficient $\alpha_{dw}(x)$ inside the separatrix. We speculate that a radial barrier to turbulent blob formation, set by the dominance of drift-wave dynamics in the core, determines the characteristic radial mode structure of the interchange turbulence. This in turn favors a specific poloidal wavenumber for the turbulence, which is manifest as the QC mode. Clearly, confirming this speculation will require more work, and is a subject of ongoing studies.

[1]Y. Takase, R. L. Boivin, F. Bombarda, P. T. Bonoli, C. Christensen, C. Fiore, D. Garnier, J. A. Goetz, S. N. Golovato, R. Granetz, M. Greenwald, S. F. Horne, A. Hubbard, I. H. Hutchinson, J. Irby, B. LaBombard, B. Lipschultz, E. Marmar, M. May, A. Mazurenko, G. McCracken, P. O'Shea, M. Porkolab, J. Reardon, J. Rice, C. Rost, J. Schachter, J. A. Snipes, P. Stek, J. Terry, R. Watterson, B. Welch, and S. Wolfe, Phys. Plasmas **4**, 1647 (1997).
[2]M. Greenwald, R. Boivin, P. Bonoli, R. Budny, C. Fiore, J. Goetz, R. Granetz, A. Hubbard, I. Hutchinson, J. Irby, B. LaBombard, Y. Lin, B. Lipschultz, E. Marmar, A. Mazurenko, D. Mossessian, T. Sunn Pedersen, C. S. Pitcher, M. Porkolab, J. Rice, W. Rowan, J. Snipes, G. Schilling, Y. Takase, J. Terry, S. Wolfe, J. Weaver, B. Welch, and S. Wukitch, Phys. Plasmas **6**, 1943 (1999).
[3]A. E. Hubbard, R. L. Boivin, R. S. Granetz, M. Greenwald, J. W. Hughes, I. H. Hutchinson, J. Irby, B. LaBombard, Y. Lin, E. S. Marmar, A. Mazurenko, D. Mossessian, E. Nelson-Melby, M. Porkolab, J. A. Snipes, J. Terry, S. Wolfe, S. Wukitch, B. A. Carreras, V. Klein, and T. S. Pedersen, Phys. Plasmas **8**, 2033 (2001).
[4]B. LaBombard, J. L. Terry, J. W. Hughes, D. Brunner, J. Payne, M. L. Reinke, I. Cziegler, R. Granetz, M. Greenwald, I. H. Hutchinson, J. Irby, Y. Lin, B. Lipschultz, Y. Ma, E. S. Marmar, W. L. Rowan, N. Tsujii, G. Wallace, D. G. Whyte, S. Wolfe, S. Wukitch, G. Wurden, and Alcator C-Mod Team, Phys. Plasmas **18**, 056104 (2011).
[5]O. E. Garcia, V. Naulin, A. H. Nielsen, and J. J. Rasmussen, Phys. Plasmas **12**, 062309 (2005).
[6]O. E. Garcia, J. Horacek, R. A. Pitts, A. H. Nielsen, W. Fundamenski, J. P. Graves, V. Naulin, and J. J. Rasmussen, Plasma Phys. Controlled Fusion **48**, L1 (2006).
[7]O. E. Garcia, J. Horacek, R. A. Pitts, A. H. Nielsen, W. Fundamenski, V. Naulin, and J. J. Rasmussen, Nucl. Fusion **47**, 667 (2007).
[8]W. Fundamenski, O. E. Garcia, V. Naulin, R. A. Pitts, A. H. Nielsen, J. J. Rasmussen, J. Horacek, J. P. Graves, and JET EFDA Contributors, Nucl. Fusion **47**, 417 (2007).
[9]D. A. Russell, J. R. Myra, and D. A. D'Ippolito, Phys. Plasmas **16**, 122304 (2009).

[10]J. R. Myra, D. A. Russell, D. A. D'Ippolito, J.-W. Ahn, R. Maingi, R. J. Maqueda, D. P. Lundberg, D. P. Stotler, S. J. Zweben, J. Boedo, M. Umansky, and NSTX Team, Phys. Plasmas **18**, 012305 (2011).
[11]S. I. Krasheninnikov, Phys. Lett. A **283**, 368 (2001).
[12]D. A. D'Ippolito, J. R. Myra, and S. I. Krasheninnikov, Phys. Plasmas **9**, 222 (2002).
[13]P. H. Diamond, S.-I. Itoh, K. Itoh, and T. S. Hahm, Plasma Phys. Controlled Fusion **47**, R35 (2005).
[14]S. I. Krasheninnikov, D. A. D'Ippolito, and J. R. Myra, J. Plasma Phys. **74**, 679 (2008).
[15]M. Wakatani and A. Hasagawa, Phys. Fluids **27**, 611 (1984).
[16]D. A. Russell, J. R. Myra, and D. A. D'Ippolito, Phys. Plasmas **16**, 122304 (2009).
[17]J. R. Angus, M. V. Umansky, and S. I. Krasheninnikov, Phys. Rev. Lett. **108**, 215002 (2012).
[18]J. R. Angus and S. I. Krasheninnikov, Phys. Plasmas **19**, 052504 (2012).
[19]R. M. McDermott, B. Lipschultz, J. W. Hughes, P. J. Catto, A. E. Hubbard, I. H. Hutchinson, R. S. Granetz, M. Greenwald, B. LaBombard, K. Marr, M. L. Reinke, J. E. Rice, D. Whyte, and Alcator C-Mod Team, Phys. Plasmas **16**, 056103 (2009).
[20]S. T. Zalesak, J. Comp. Phys. **31**, 331 (1979) and references therein.
[21]D. A. D'Ippolito, J. R. Myra, and S. J. Zweben, Phys. Plasmas **18**, 060501 (2011).
[22]R. J. Goldston, Nucl. Fusion **52**, 013009 (2012).
[23]See the discussion in Sec. VI.A.5 of Ref. 21 and references therein.